JOURNAL OF AIRCRAFT
Vol. 43, No. 4, July–August 2006

Study of the Residual Strain in Lap Joints

Gang Li,* Guoqin Shi,† and Nicholas C. Bellinger‡
National Research Council Canada, Ottawa, Ontario K1A 0R6, Canada

Both experiments and finite element analysis were carried out to study the residual strain (stress) in the riveted lap joint for a better understanding of the fatigue life of fuselage lap joints. A force-controlled riveting process was used to apply a constant load ramp to install the rivets. Strain variations on the joint surface were measured using microstrain gauges during the riveting process. Because neutrons are known to penetrate through many centimeters of aluminum alloys, neutron diffraction was used to provide a nondestructive technique to determine strains at certain depths in the joint. Parallel to the experimental testing, a two-dimensional axisymmetric finite element model was developed to simulate the riveting process. Both material and geometric nonlinearities, as well as nonlinear contact boundary conditions, were used in this numerical model. Comparisons between the numerical simulations and experimental results focused on the rivet driven head deformations and strain variations, and the results showed that the current two-dimensional axisymmetric finite element model using the proper boundary conditions can reliably be used to determine the residual strains (stresses) present in joints that were induced during the riveting process.

Nomenclature

C	=	material parameter
D	=	rivet shank diameter
$D_{\max}$	=	maximum rivet shank diameter after riveting
d	=	spacing between lattice plane
d_0	=	stress-free lattice spacing
E	=	Young's modulus
m	=	material parameter
r	=	distance to fastener hole centre
ε	=	normal strain
$\varepsilon_{\text{true}}$	=	true strain
θ	=	diffracted neutrons' angle
λ	=	wavelength of the incident neutron beam
ν	=	Poisson's ratio
σ	=	normal stress
σ_{true}	=	true stress beyond the initial yield stress
σ_y	=	initial yield stress

I. Introduction

RIVETED fuselage lap joints have been widely used in the aeronautical industry for many years. The fatigue and static strength of joints are strongly influenced by the residual stress and strain induced by the riveting process.[1–3] To understand joint integrity, it is necessary to study the localized conditions of residual stress and strain at and around the rivet/hole interface generated during the rivet installation process. Previous research that has been carried out to determine the residual stress and strain in riveted lap joints used theoretical, experimental, and numerical methods.[1–18] Because of the complexity associated with the riveting process, it is difficult to develop a closed-form theoretical solution. Experimental testing and finite element methods have been used to determine the stress state present in lap joints.

Riveting of fuselage lap joints using a quasi-static force-controlled method have been carried out in the past[13–17] to better control the rivet installation and, thus, the consistency of the conditions at and around the rivet/sheet hole interface.[1–3] Both microstrain gauges and neutron diffraction were used to understand the strain variations in joints during and after the riveting process. Because microstrain gauges are capable of capturing the strain variations on a lap joint surface during the riveting process, the variation in the load history can be determined.[10,11,14,16] The microstrain gauge method is convenient, cheap, and reliable; however, it can only determine the strain variation at the surface. Because neutrons penetrate many centimeters through aluminum alloys, neutron diffraction has been used as a nondestructive technique to measure the internal strains present in aluminum components.[17,18] However, it is difficult to use neutron diffraction to measure in situ strain variations in joints during the riveting process, and, thus, this method was used after the riveting process was completed. In addition to the experimental tests, a two-dimensional axisymmetric finite element (FE) model was developed to simulate the residual stress and strain in joints induced by the riveting process.[15–17] Material and geometry nonlinear properties, as well as the contact situations, were considered in the numerical simulation. The strain variations measured from both microstrain gauges and neutron diffraction were used to verify the numerical model. Once the FE model was validated, the variations in the rivet driven head deformations, the in situ stress and strain conditions at any position within the lap joint, as well as the full-field stress and strain contours were extracted from the FE results to obtain the residual stress and strain distributions that were present in the riveted lap joint.

II. Experimental Details

The specimen configuration used in this study is shown in Fig. 1 and consisted of two 76.20×76.20 mm bare 2024-T3 Al alloy sheets, each 2.03 mm thick, and one 2117-T4 Al alloy countersunk type rivet, MS20426AD8-9 (Ref. 19). The rivet had a total length of 14.29 mm and shank diameter D of 6.35 mm. The mean inner sheet hole diameter was 6.45 mm, and the rivet mean protruding height above the inner sheet surface was 9.95 mm based on the optical measurement results of 20 specimens.[14,16] In the current study, three joint specimens: one microstrain-gauged specimen and two nongauged specimens, were tested using a 53.38-kN squeeze force. To avoid both the thermal and inertial influence on the specimen, a small constant loading ramp of 111.2 N/s was chosen for the riveting tests, which is very slow compared to the actual rivet loading rates. After the tests were completed, one riveted and one unriveted specimen

Received 9 June 2005; revision received 27 October 2005; accepted for publication 10 November 2005.

*Research Officer, Structures and Materials Performance Laboratory, Institute for Aerospace Research, 1200 Montreal Road; Gang.Li@nrc-cnrc.gc.ca. Member AIAA.

†Senior Research Officer, Structures and Materials Performance Laboratory, Institute for Aerospace Research, 1200 Montreal Road. Member AIAA.

‡Structures Group Leader, Structures and Materials Performance Laboratory, Institute for Aerospace Research, 1200 Montreal Road. Member AIAA.

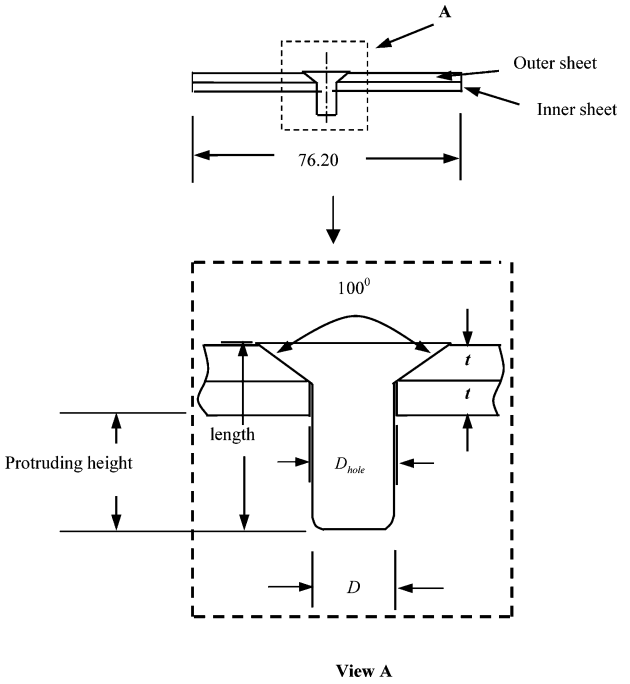

Fig. 1 Specimen geometry (millimeters).

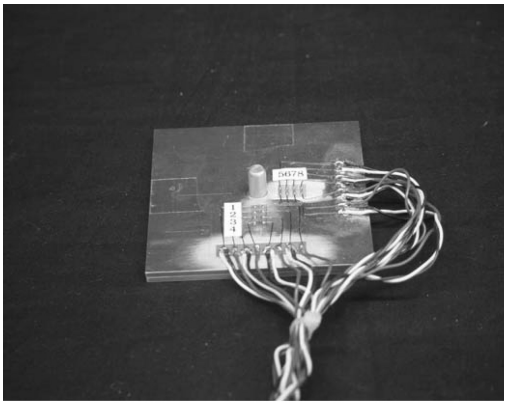

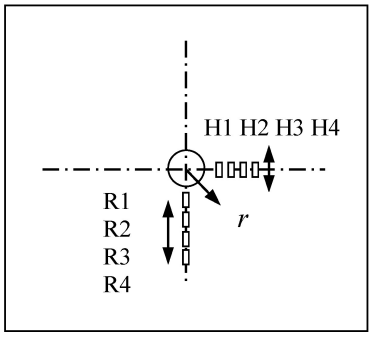

Fig. 2 Microstrain gauge arrangement on inner sheet surface before riveting.

(strain/stress-free joint) were sent to Chalk River Laboratory of the Steacie Institute for Molecular Science, National Research Council Canada, to measure the residual strains in the riveted lap joint using neutron diffraction.

A. Microstrain Gauge Measurement

In situ measurements of the strain variation in both the radial and hoop (tangential) directions were obtained during the riveting process using the microstrain gauges.[14,16] Figure 2 shows the microstrain gauge arrangement on the joint inner sheet surface. By defining the radial coordinate value of r to be zero at the joint hole center, the strain gauge locations can be identified. Gauges R1–R4 were located at $r = 7.85$, 10.55, 13.35, and 16.15 mm, whereas gauges H1–H4 were at positions $r = 7.88$, 10.35, 12.86, and 15.38 mm. Gauges R1–R4 (micro-measurements EA-13-031EC-350 with gauge factor of $2.09 \pm 1.0\%$) were used to measure the radial strain values and gauges H1–H4 (micro-measurements EA-13-031DE-350 with gauge factor of $2.06 \pm 1.0\%$) were used to measure the hoop direction strain values.

B. Neutron Diffraction Technique

The neutron diffraction technique was carried out at the Chalk River Laboratory of the National Research Council Canada to measure the internal strains. At this laboratory, neutrons are generated using a nuclear reactor and then directed toward the location of interest on the specimen where they are diffracted from the lattice planes of the crystallites that form the material. The angle 2θ, at which the neutrons are diffracted, depends on the wavelength of the incident neutron beam λ and the spacing between the lattice planes d through Bragg's law in Eq. (1):

$$\lambda = 2d \sin(\theta) \tag{1}$$

The lattice strain ε is the fractional change in the lattice spacing d with reference to the stress-free lattice spacing d_0 in Eq. (2),

$$\varepsilon = (d - d_0)/d_0 \tag{2}$$

By aligning the specimen in the proper direction, the strain in the x, y, and z directions can be determined. The normal stress σ in these directions can be estimated from these three strain components.

The incident and diffracted neutron beams are shaped by slits cut in the neutron-absorbing cadmium masks. The nominal volume defined by the intersection of these rectangular cross-section beams is called the instrumental gauge volume. Measurements were taken along a scan line parallel to the y axis. The goal was to obtain data close to the rivet/sheet and sheet/sheet interfaces. However, fine spatial resolution required a commensurately small instrumental gauge volume. Aluminum sheet has a relatively small coherent cross section for neutron measurements, imposing a lower limit of approximately 1 mm^3 on the volume of the gauge to obtain data of sufficient statistical quality for the number of data points provided in the allotted time. Two gauge geometries were, therefore, required. For the measurements of the x and y components of strain, the gauge dimensions were $0.5 \times 0.5 \times 5$ mm^3 with the 5-mm dimension parallel to z and a diamond cross section in the x–y plane. For the z (hoop) component, the dimensions were $1 \times 1 \times 1$ mm^3 with a rectangular cross section in the x–z plane. The setup of a riveted lap joint using neutron diffraction measurement is shown in Fig. 3. Figure 4 shows the neutron diffraction measurement locations in the joint. These were 5.7, 6.7, 7.7, 10, and 20 mm from the rivet center for the outer sheet and 3.6, 4.6, 5.6, 10, and 20 mm from the rivet center for the inner sheet.[17,18]

III. FE Simulation

A. Material Parameters

The elastic–plastic properties for the material used in the FE modeling were obtained from uniaxial tensile tests of 2.03-mm-thick bare 2024-T3 Al alloy sheet.[14,19] The material properties used for the bare sheet were $E = 72.4$ GPa, $\nu = 0.33$, and $\sigma_y = 310$ MPa (initial yield stress), whereas these used for the 2117-T4 Al alloy rivet[2,3] were $E = 71.7$ GPa, $\nu = 0.33$, and $\sigma_y = 172$ MPa (initial yield stress).

Curve fitting expressions for both the sheet and rivet were used when the true stress was beyond the initial yield stress, which was determined using Eq. (3)

$$\sigma_{\text{true}} = C(\varepsilon_{\text{true}})^m \tag{3}$$

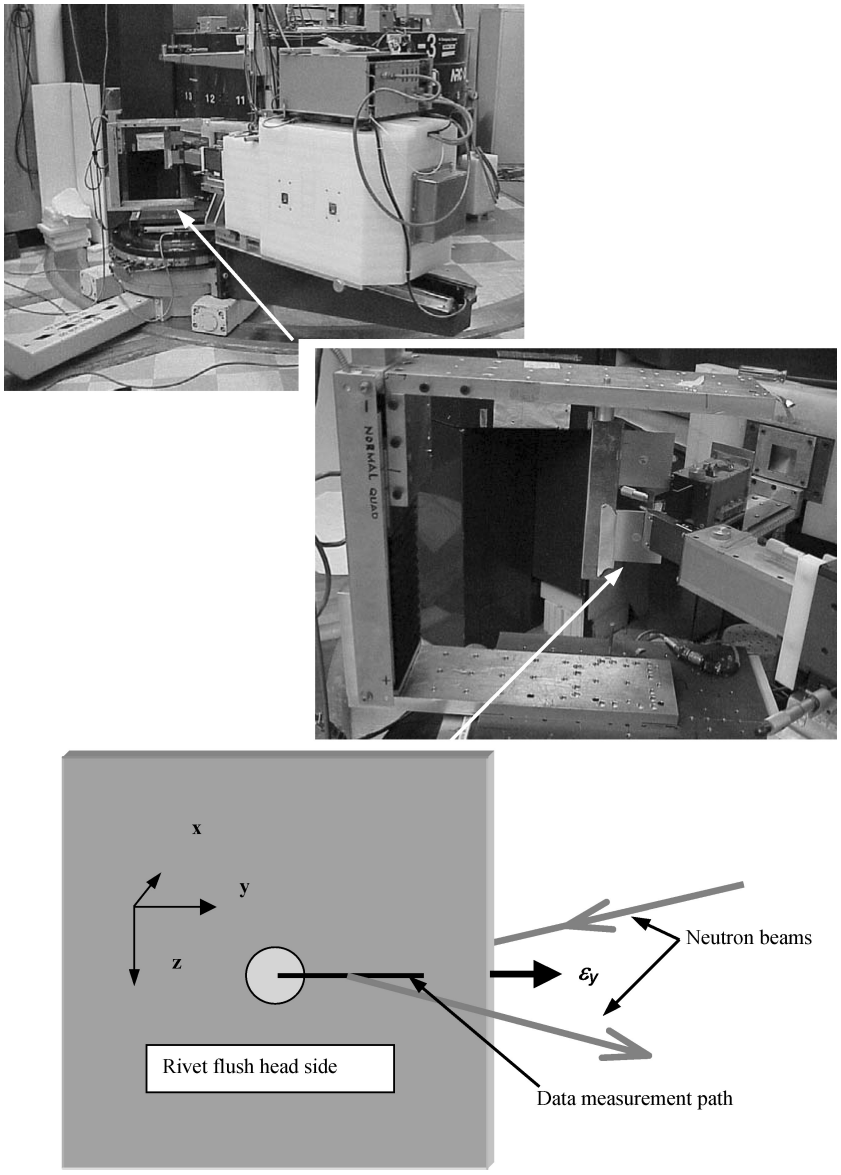

Fig. 3 Setup of riveted lap joint for neutron diffraction measurement.

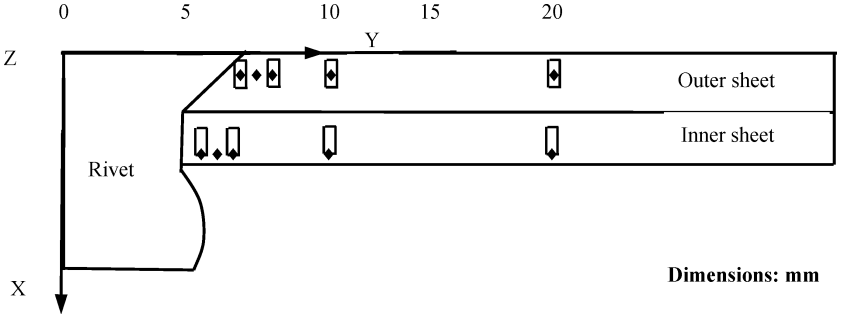

Fig. 4 Schematic of gauge location, dimension, and orientation for □, hoop strain ε_z and ◇, radial and clamping strains ε_y and ε_x in riveted lap joint using neutron diffraction technique.

where σ_{true} is the true stress, $\varepsilon_{\text{true}}$ is the true strain, and C and m are material parameters.

The hardening parameters used for the sheet were $C = 765.67$ MPa and $m = 0.14$ when $\varepsilon_y < \varepsilon_{\text{true}} \leq 0.02$ (ε_y was the initial yield strain), $C = 744.62$ MPa and $m = 0.164$ when $0.02 < \varepsilon_{\text{true}} \leq 0.10$, and the slope of the linear hardening curve was 1.034 GPa when $\varepsilon_{\text{true}} > 0.10$. The hardening parameters used for the rivet were $C = 544$ MPa and $m = 0.23$ when $0.02 < \varepsilon_{\text{true}} \leq 0.10$ and $C = 551$ MPa and $m = 0.15$ when $0.10 < \varepsilon_{\text{true}} \leq 1.0$.

A tabular listing of the stress and plastic strain values were input into a table provided by MSC.Patran interface, which used linear interpolation for values between the points to implement the hardening behavior of the model. Isotropic hardening behavior was assumed for both the rivet and sheet materials.

B. FE Modeling

A two-dimensional FE model (FEM) was used to study the residual stress and strain distributions induced by the riveting

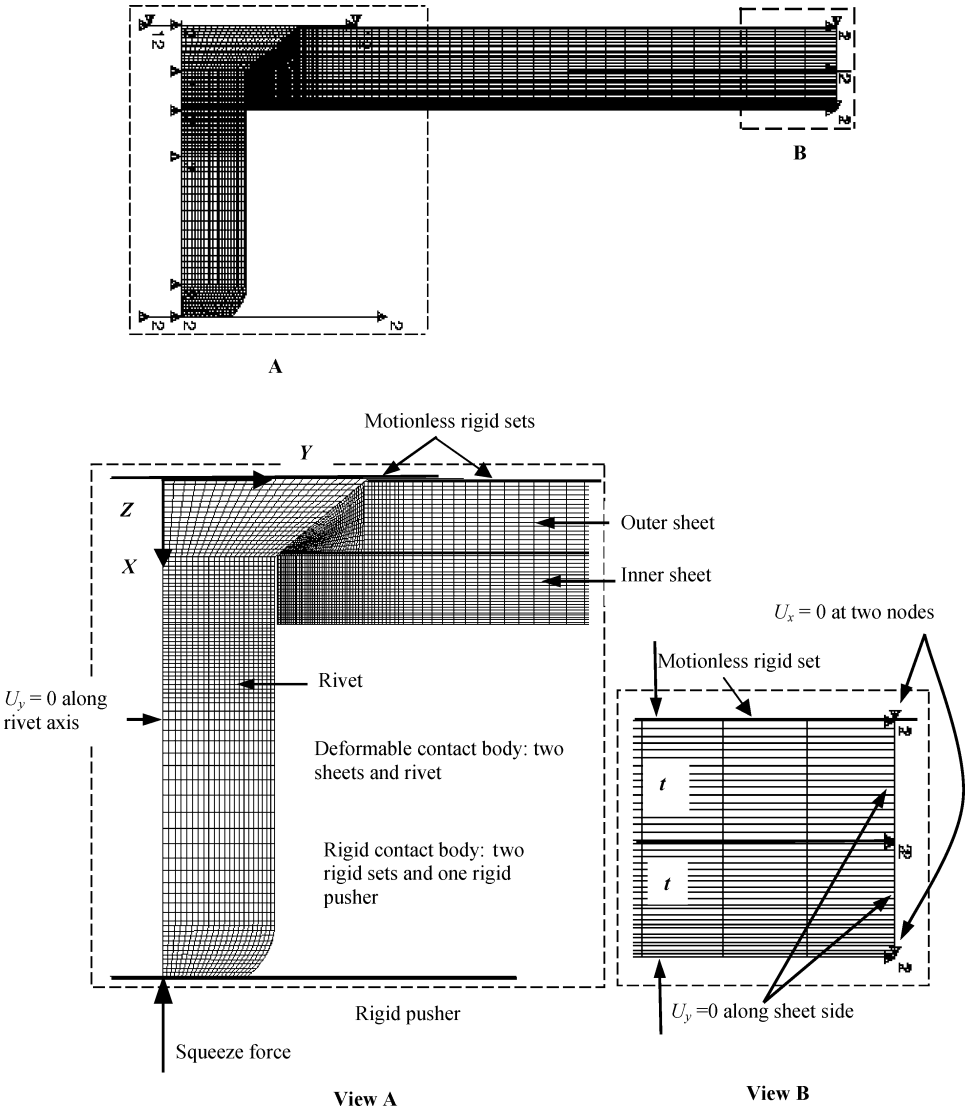

Fig. 5 Schematic diagram of two-dimensional axisymmetric FE model with three deformable contact bodies, three rigid contact bodies, and the FEM mesh and boundary conditions of set 2 for simulation of lap joint.

process.[15–17] MSC.Patran and MSC.Marc were used to carry out the analysis. Different mesh sizes were examined to determine the convergence of the rivet deformation and the maximum rivet shank diameter deformation ratio of $D_{\max}/D$, where D is the rivet shank diameter before riveting and $D_{\max}$ is the maximum rivet shank diameter after riveting. A very fine mesh was chosen from this study with a total of 5410 nodes and 5099 elements of four-node axisymmetric elements with reduced integration. The mesh for the sheets extended to five rivet shank diameters ($5D$) from the joint symmetric axis x as shown in Fig. 5. The squeeze force was applied to the rigid pusher, which compressed the rivet driven head edge. A coefficient of friction of 0.2 was chosen between all contact bodies and friction was modeled using a coulomb model.[8–11,13,15–17]

Two different sets of boundary conditions were used in the two-dimensional axisymmetric FEM[15]:

For set 1, radial displacement $U_y = 0$ was applied at the rivet axis and the far ends of the sheets. A vertical displacement $U_x = 0$ was applied at the two corner points of the outer side edge. One rigid set supported the rivet bottom and one rigid pusher was used to squeeze the rivet driven head.

For set 2, the third rigid body was introduced to support the external surface of the outer sheet on the basis of the boundary conditions in set 1, as shown in Fig. 5.

The outer sheet surface did not touch the bottom rigid set during the riveting process if the FEM used the boundary conditions in set 1, which was only an idealized case. To simulate more accurately actual testing conditions and to improve set 1, the joint outer sheet touched the third rigid body located at the joint bottom during the riveting process in set 2.

IV. Results and Discussion

The following results were analyzed based on the FEM coordinate frame, where x is in the sheet thickness direction, y is in the radial direction, and z is in the hoop direction.

Very little difference was found for the rivet deformations obtained from the numerical model using the displacement boundary conditions from sets 1 and 2. Variations in the rivet driven head compressive displacement vs the squeeze force during the riveting process are presented in Fig. 6. It can be seen from Fig. 6 that the experimental results and the FE predictions agreed very well. The rivet diameter deformation ratio of $D_{\max}/D$ was 1.70 for both the experimental and numerical results.[14–17] Figure 7 shows the unriveted and riveted specimens.[14,15]

A. Comparison of Microstrain Gauge Results with FEM Predictions for Sheet Strain Variations During the Riveting Process

Comparisons of the strain variations obtained from the experimental tests and FEM for the radial and hoop directions are presented in Figs. 8 and 9, respectively. Note from Figs. 8 and 9 that during

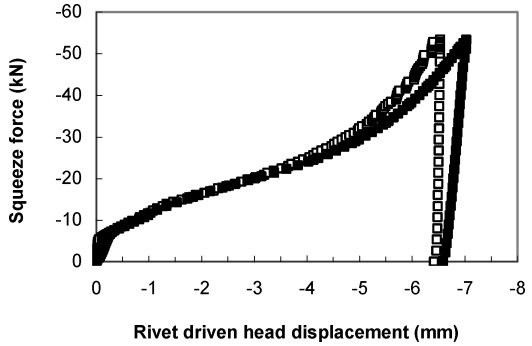

Fig. 6 Comparison of rivet driven head displacement during entire riveting period using 53.38-kN rivet squeeze force determined by experimental test and FE method using displacement boundary conditions of set 1 or 2: □, FE, $F = -53.38$ kN and ■, experiment, $F = -53.38$ kN.

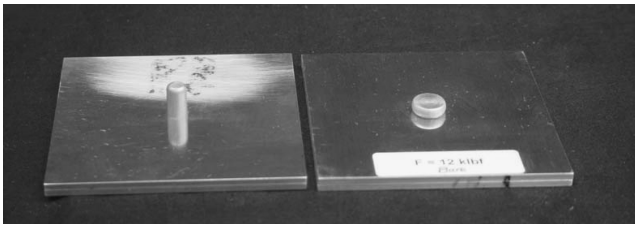

a) Photographs of joint before riveting and after riveting using 53.38-kN squeeze force

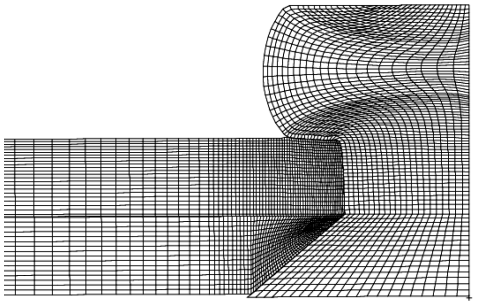

b) FEM prediction of rivet driven head shape riveted at 53.38-kN squeeze force

Fig. 7 Rivet driven head shape obtained from experiment and FEM analysis.

the riveting process compressive strains were present in the radial direction, whereas tensile strains were present in the hoop/tangential direction. Comparisons between the strain variation trends showed good agreement between the FEM and experimental results for all of the strain pairs except for a small portion during the entire riveting period. The numerical simulation resulted in excellent predictions for the hoop strain but was less accurate for the radial strain. Figures 8 and 9 show that the numerical model that used the boundary condition in set 2 gave more accurate results than the boundary condition in set 1. A total of six contact bodies were used in set 2 whereas five contact bodies were used in set 1. The three rigid contact bodies were two rigid sets and one rigid pusher, whereas the three deformable contact bodies were the two sheets and one rivet. In the case of set 1, the radial displacement of the sheets near the rivet was larger than that for set 2 because its movement was only constrained by the countersunk head. The large plastic deformation in the rivet driven head side led to certain sheet bending; thus, relatively large radial strains occurred, whereas the sheet bending could be effectively decreased or avoided in set 2 conditions. The radial strains on the inner sheet surface from set 2 conditions should be less than those of set 1. From the experimental point of view, the boundary conditions of set 2 were more accurate than those of set 1.

The discrepancy in the radial strain between the microstrain gauge results and FEM predictions are also found elsewhere[10,11] and can be explained as follows: 1) The constitutive models for the sheet and rivet used in the FEM could be inaccurate. 2) The material properties and surface were assumed perfect in the FEM, which is unrealistic. 3) The friction model used for the contact interface in the FEM could be inaccurate. 4) Numerical errors were present in the FEMs. 5) The errors were associated with the strain gauge, for example, gauge reliability and gauge bond condition. The experimental uncertainty in strain measurements could be very high.[20]

B. Comparison of Neutron Diffraction Measurements with FEM Predictions

Comparisons between the strain distributions in the radial, hoop, and clamping directions from the neutron diffraction technique and the FEM using the boundary conditions in set 2 are presented in Figs. 10 and 11 for the outer sheet and the inner sheet, respectively. Upper and lower bounds for the strain values obtained from the neutron diffraction technique are also presented in Figs. 10 and 11. Note that the depths for the data point for ε_x (or ε_y) and ε_z inside the outer sheet were different due to the measurement adjustment of the gauge center. A reasonable agreement was achieved between the neutron diffraction results and the numerical predictions.

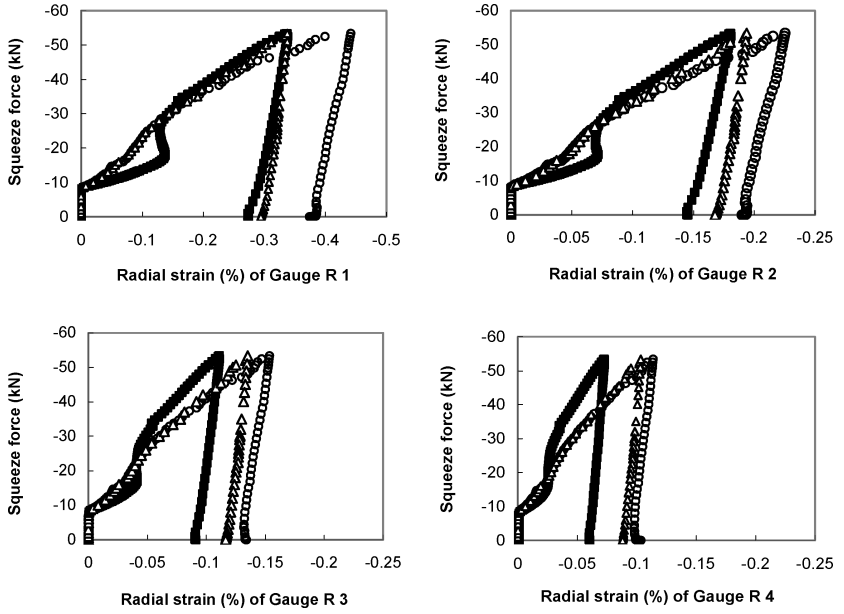

Fig. 8 Comparison of radial strain variations in gauges R1–R4 on inner sheet surface during riveting process under 53.38-kN squeeze force obtained from microstrain gauge and two-dimensional FEM results: ■, microstrain gauge result; ○, FEM prediction using BC set 1; and △, FEM prediction using BC set 2.

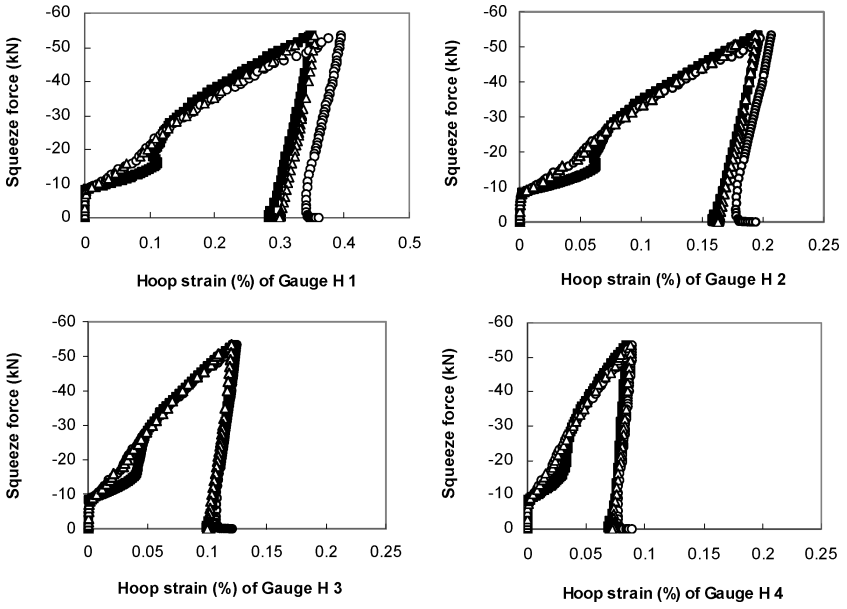

Fig. 9 Comparison of hoop strain variations in gauges H1–H4 on inner sheet surface during riveting process under 53.38-kN squeeze force obtained from microstrain gauge and two-dimensional FEM results: ■, microstrain gauge result; ○, FEM prediction using BC set 1; and △, FEM prediction using BC set 2.

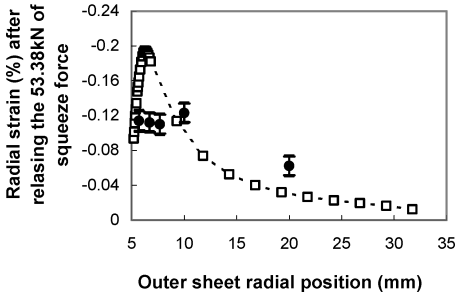

a) Radial strain: --□--, FEM, radial strain at $x = 0.5$ mm and ●, neutron data

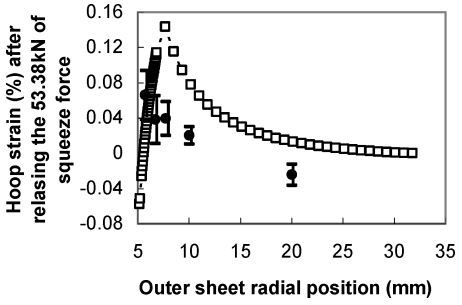

b) Hoop strain: --□--, FEM, hoop strain at $x = 1.1$ mm and ●, neutron data

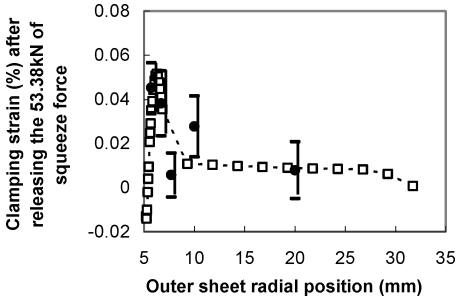

c) Clamping strain: --□--, FEM, clamping strain at $x = 0.5$ mm and ●, neutron data

Fig. 10 Comparison of residual strains in outer sheet along radial position predicted by numerical method and neutron diffraction after unloading 53.38–kN squeeze force.

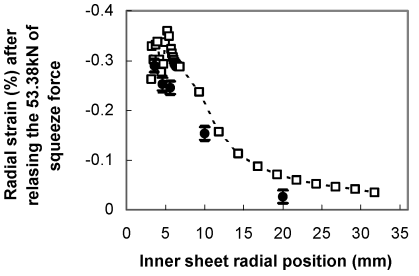

a) Radial strain: --□--, FEM, radial strain at $x = 3.1$ mm and ●, neutron data

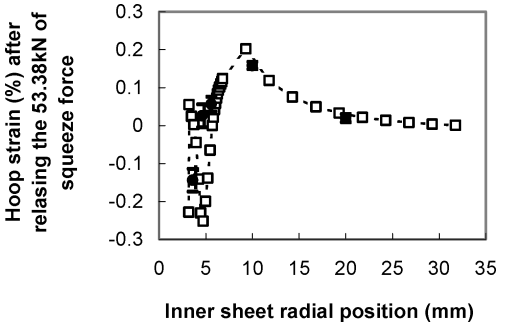

b) Hoop strain: --□--, FEM, hoop strain at $x = 3.1$ mm and ●, neutron data

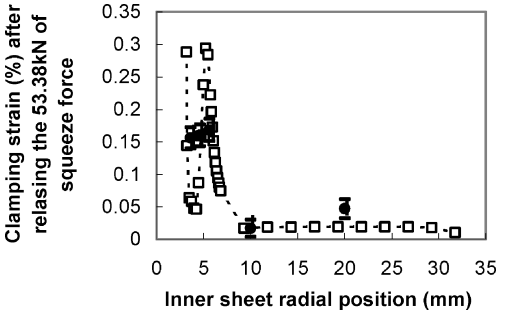

c) Clamping strain: --□--, FEM, clamping strain at $x = 3.1$ mm and ●, neutron data

Fig. 11 Comparison of residual strains in inner sheet along radial position predicted by numerical method and neutron diffraction after unloading 53.38-kN squeeze force.

The discrepancy in the results could be caused by the following: 1) The gauge used for the neutron diffraction measurement had a specific volume, instead of a point, and, thus, the strain data were averaged,[17,18] whereas the strain values determined from the numerical results were obtained from nodes (point values). 2) Differences in the gauge locations existed between the neutron diffraction technique and the numerical model. 3) Errors could have been present during the experiment and joint manufacturing, as well as in the numerical analysis, for example, materials properties.

V. Summary

The following conclusions can be drawn from this study:

1) A two-dimensional axisymmetric FEM was developed and used to carry out a nonlinear analysis to simulate the residual stress/strain resulting from the riveting process used to manufacture fuselage lap joints.

2) Experimental studies of the riveting process were performed, and the strain variations were measured using microstrain gauges.

3) The neutron diffraction technique was used to measure the residual strains inside the skins of the riveted lap joint, which cannot be determined using strain gauges.

4) The radial and hoop strains obtained from either the in situ strain gauges or the neutron diffraction technique compared reasonably well with the FE results. Therefore, the residual stresses could be obtained using the developed two-dimensional FEM for any location within a lap joint or at any loading.

Acknowledgments

This work has been carried out under Institute for Aerospace Research Program 303 Aerospace Structures, Project 46_QJ0_37, Residual Stress in Riveted Lap Joints. The financial assistance received from Department of National Defence/Defence Research and Development Canada is gratefully acknowledged. Thanks are also extended to J. P. Komorowski and G. Eastaugh for their valuable discussions, suggestions, and help in this research.

References

[1]Müller, R. P. G., "An Experimental and Analytical Investigation on the Fatigue Behavior of Fuselage Riveted Lap Joints," Ph.D. Dissertation, Faculty of Aerospace Engineering, Delft Univ. of Technology, Delft, The Netherlands, Oct. 1995.

[2]Szolwinski, M. P., "The Mechanics and Tribology of Fretting Fatigue with Application to Riveted Lap Joints," Ph.D. Dissertation, School of Aeronautics and Astronautics, Purdue Univ., West Lafayette, IN, Aug. 1998.

[3]Szolwinski, M. P., and Farris, T. N., "Linking Riveting Process Parameters to the Fatigue Performance of Riveted Aircraft Structures," *Journal of Aircraft*, Vol. 37, No. 1, 2000, pp. 130–137.

[4]Schütz, Z., "Endurance of Single Shear Light Alloy Riveted Joints," LBF, Bericht Nr. F-47, 1963 (in German).

[5]Donaldson, D. R., and Kenworthy, K. J., "Fatigue Design and Test Program for the American SST," *Aircraft Fatigue Design, Operational and Economics Aspects*, edited by J. Y. Mann and I. S. Milligan, Pergamon, Rushcutters Bay, 1972, pp. 437–476.

[6]Ryzhova, T. B., "Estimation of the Reliability of Ultrasonic Quality Control of Riveted Joints with Clearance," *Russian Journal of Nondestructive Testing*, Vol. 30, No. 6, 1994, pp. 418–421.

[7]Ryzhova, T. B., "Ultrasonic Assessment of the Radial Clearance of Riveted Joints in Aircraft Structures," *Proceedings of 21st International Council of Aeronautical Sciences Congress*, Paper ICAS-98-R, 4,2, Sept. 1998, pp. 1–7.

[8]Fitzgerald, T. J., and Cohen, J. B., "Residual Stresses in and Around Rivets in Clad Aluminum Alloy Plates," *Materials Science and Engineering*, Vol. A188, No. 1-2, 1994, pp. 51–58.

[9]Slater, W. J., "Static Strength of Riveted Joints in Fiber Metal Laminates," Ph.D. Dissertation, Faculty of Aerospace Engineering, Delft Univ., Delft, The Netherlands, April 1994.

[10]Markiewicz, E., Langrand, B., Deleotombe, E., Drazetic, P., and Patronelli, L., "Analysis of the Riveting Forming Mechanisms," *International Journal of Materials and Product Technology*, Vol. 13, No. 3–6, 1998, pp. 123–145.

[11]Langrand, B., Patronelli, L., Deleotombe, E., Markiewicz, E., and Drazetic, P., "An Alternative Numerical Approach for Full Scale Characterization for Riveted Joint Design," *Aerospace Science and Technology*, Vol. 6, No. 5, 2002, pp. 343–354.

[12]Li, G., and Shi, G., "Residual Stresses in Riveted Lap Joints: A Literature Review," Inst. for Aerospace Research, LTR-SMPL-2002-0019, National Research Council Canada, 2002.

[13]Li, G., and Shi, G., "Nonlinear Finite Element Analysis of Residual Stresses in Riveted Lap Joints with Protruding Head Rivet," Inst. for Aerospace Research, LTR-SMPL-2002-0249, National Research Council Canada, 2002.

[14]Li, G., and Shi, G., "Investigation of Residual Stress in Riveted Lap Joints: Experimental Study," Inst. for Aerospace Research, LTR-SMPL-2003-0099, National Research Council Canada, 2002.

[15]Li, G., and Shi, G., "Investigation of Residual Stress in Riveted Lap Joints: Numerical Simulation Study," Inst. for Aerospace Research, LTR-SMPL-2003-0101, National Research Council Canada, 2003.

[16]Li, G., and Shi, G., "Effects of the Riveting Process on the Residual Stress in Fuselage Lap Joints," *Canadian Aeronautics and Space Journal*, Vol. 50, No. 2, 2004, pp. 91–105.

[17]Li, G., Shi, G., and Bellinger, N. C., "Neutron Diffraction Measurement and FE Simulation of Residual Strains in Fuselage Lap Joints," Inst. for Aerospace Research, LTR-SMPL-2004-0003, National Research Council Canada, 2004.

[18]Rogge, R. B., "Strain and Stress Distribution in Riveted Lap Joints," NPMR-ANDI-168, Steacie Inst. for Molecular Sciences at Chalk River, National Research Council Canada, 2003.

[19]"Metallic Material and Elements for Aerospace Vehicle Structures," MIL-HDBK-5H, U.S. Dept. of Defense, Dec. 1998.

[20]Li, G., and Lee-Sullivan, P., "Finite Element and Experimental Studies on Single-Lap Balanced Joints in Tension," *International Journal of Adhesion and Adhesives*, Vol. 21, No. 3, 2001, pp. 211–220.